THE JOURNAL OF PHYSICAL CHEMISTRY LETTERS
A JOURNAL OF THE AMERICAN CHEMICAL SOCIETY

pubs.acs.org/JPCL

Letter

Monitoring Strain-Controlled Exciton–Phonon Coupling in Layered MoS_2 by Circularly Polarized Light

Yan Zhao, Shuqing Zhang, Bo Xu, Shishu Zhang, Shiyi Han, Jin Zhang, and Lianming Tong*

Cite This: *J. Phys. Chem. Lett.* 2021, 12, 11555–11562

Read Online

ACCESS | Metrics & More | Article Recommendations | Supporting Information

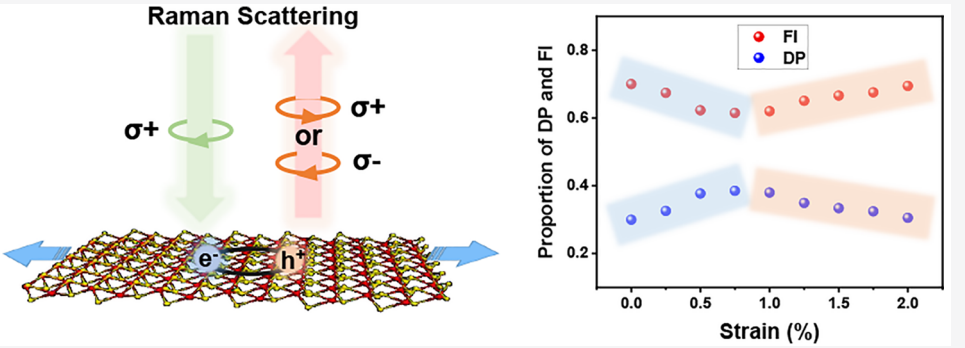

ABSTRACT: The modulation of exciton–phonon coupling by strain greatly affects the optical and optoelectronic properties of two-dimensional (2D) materials. Although photoluminescence and optical absorption spectra have been used to characterize the overall change of exciton–phonon coupling under strain, there has been no effective method to distinguish the evolution of the major contributions of exciton–phonon coupling, that is, deformation potential (DP) and Fröhlich interaction (FI). Here we report the direct monitoring of the evolution of DP and FI under strain in layered MoS_2 using circularly polarized Raman spectroscopy. We found that the relative proportions of DP and FI can be well evaluated by the circular polarization ratio of the E^1_{2g} mode for strained MoS_2. Further, we demonstrated that the strain control of DP and FI in MoS_2 is dominated by the excitonic effect. Our method can be extended to other 2D semiconductors and would be helpful for manipulating exciton–phonon couplings by strain.

Two-dimensional (2D) materials have shown vast potential in electrical and optical devices, and great efforts have been made to modify the physical properties of 2D materials in order to improve the performance. Strain engineering has been proven to be an effective approach to tune the electronic band structure, carrier mobility, and optical emission of 2D materials.[1−5] For example, the tensile strain induced enhancement of carrier mobility in monolayer MoS_2 has been reported both theoretically and experimentally.[6−8] The electron (or exciton)-phonon coupling is one of the major factors that affect the carrier mobility,[9] which is also involved in various physical processes, such as optical absorption and photoluminescence (PL),[10−12] valley scattering,[13−16] and thermal transport.[17−20] There are mainly two forms of electron/exciton–phonon couplings for polar semiconducting 2D materials, that is, the deformation potential (DP)[21] and the Fröhlich interaction (FI).[22] DP is a common form of electron/exciton–phonon coupling in materials, which comes from the crystal potential induced by the distortion of lattice, while the FI is generated by the longitudinal optical (LO) phonon of polar or ionic crystals, in which the relative motion of atoms with opposite charges can form a macroscopic electric field. The DP and FI can play different roles during their involvement in the above physical processes.[23,24] And the investigation of the DP and FI exciton–phonon coupling under strain is important for understanding the modulation of electrical and optical properties of 2D materials.

PL and optical absorption spectra have been used to explore the exciton–phonon coupling in strained transition metal dichalcogenides (TMDCs) by assuming that the line width of exciton transition is governed by exciton–phonon coupling at room temperature.[10−12,25] Moreover, by fitting the temperature-dependent line width of exciton emission, the coupling strength of exciton and phonon can be extracted.[26−28] Besides, the strength of exciton-LO phonon coupling can be quantitatively expressed by the Huang–Rays factor which is extracted from the intensity ratio of the second-order to the first-order phonon replica of the phonon-assisted luminescence.[23,29] Layered MoS_2 is a 2D semiconductor with a large exciton binding energy[30] and has been a prototype for

Received: October 24, 2021
Accepted: November 18, 2021

https://doi.org/10.1021/acs.jpclett.1c03481
J. Phys. Chem. Lett. 2021, 12, 11555–11562

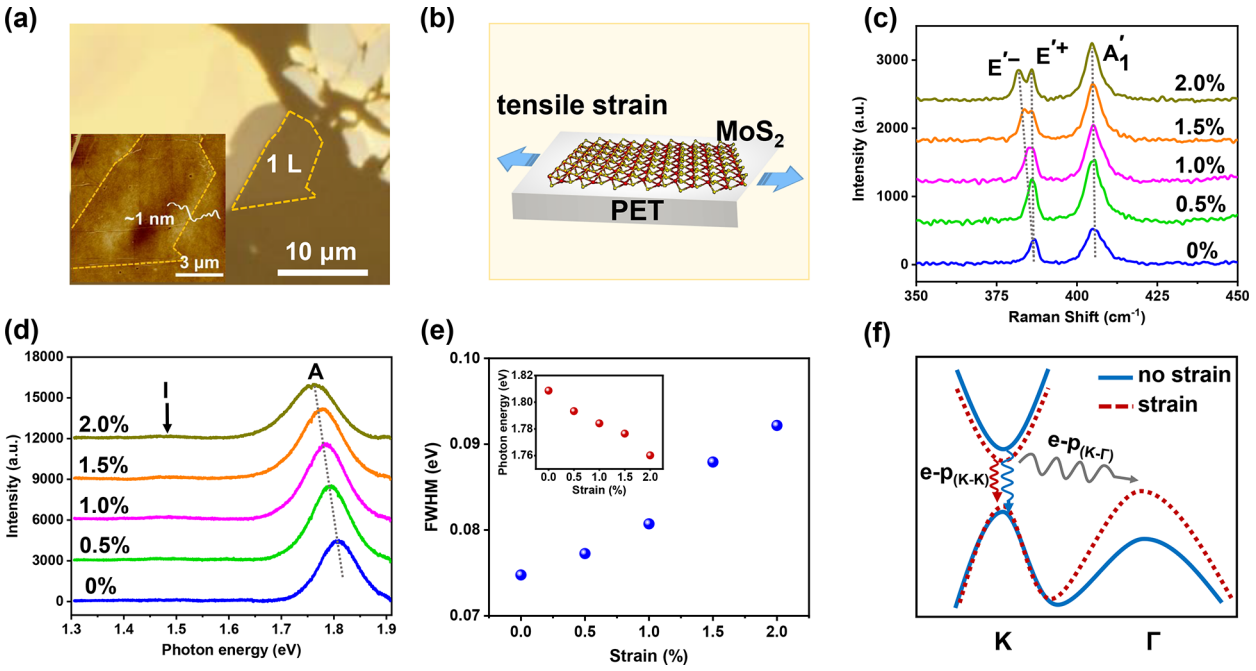

Figure 1. The Raman and PL spectra of monolayer MoS_2 under strain. (a) Optical image of the mechanically exfoliated monolayer MoS_2 flake on the PET substrate. Insets are the AFM image and the height profile of the MoS_2 flake. (b) The schematic diagram of the application of uniaxial tensile strain on the PET substrate and the MoS_2 flake. (c, d) The Raman (c) and PL spectra (d) of monolayer MoS_2 excited by a 532 nm (2.33 eV) laser with the increase of strain. (e) The variation of photon energy (inset) and full width at half-maximum (fwhm) of the A exciton emission peak as a function of strain. (f) Schematic diagram of the intravalley ($e-p_{(K-K)}$) and intervalley ($e-p_{(K-\Gamma)}$) exciton−phonon couplings in unstrained and strained monolayer MoS_2.

exploring the strain control of exciton−phonon interaction[25] owing to its prominent excitonic effects[31,32] and favorable strain responses.[33−35] However, although a series of studies have been reported on the strain engineering of layered MoS_2, the evolution of DP and FI exciton−phonon couplings under strain has not been explored yet.

Herein, we report the monitoring of different exciton−phonon couplings as a function of strain in layered MoS_2 using Raman spectroscopy excited by circularly polarized light. For the helicity-resolved Raman spectra (HRRS) of MoS_2,[36,37] the intensities of the helicity-changed and helicity-conserved components of the E^1_{2g} mode are determined by the DP and the FI, respectively. Uniaxial tensile strain was applied to mechanically exfoliated monolayer and bilayer MoS_2, and the helicity of Raman scattered light for the degenerate longitudinal (LO) and transverse (TO) optical phonon modes (E^1_{2g} mode) was measured. We first explored the helicity selection rule of strained MoS_2 for off- and on-excitonic resonance excitation, and then we demonstrated that the proportion of the DP and FI can be extracted from the ratio of helicity-changed to helicity-conserved components of the E^1_{2g} mode both for the unstrained and strained MoS_2. We found that the variation of the proportion of the DP and FI with strain is dominated by the excitonic resonance effect, and the FI is more sensitive to strain due to the excitonic effect compared with the DP.

Monolayer MoS_2 was mechanically exfoliated onto the flexible polyethylene terephthalate (PET) substrate, and the thickness of the MoS_2 flake characterized by atomic force microscope (AFM) is ~1 nm, as shown in Figure 1a. The uniaxial tensile strain is applied by stretching the PET substrate (Figure 1b), as has been widely used in the literature.[38,39] The strain can be calculated according to the deformation of the PET substrate. It should be noted that although the effective strain applied to MoS_2 is typically slightly smaller than that to the PET, we still use the apparent experimental strain in this work since the strain transfer efficiency from PET to MoS_2 is expected to be more than 90%, which is related to the Young's modulus of PET (>1 GPa).[40,41]

The Raman spectra of MoS_2 excited by 532 nm laser (2.33 eV) with the increase of strain are shown in Figure 1c. There are two first-order Raman active modes in backscattering configuration for MoS_2, that is, the in-plane E^1_{2g} mode (E′ mode for monolayer) and the out-of-plane A_{1g} mode (A_1' mode for monolayer).[42] The degenerate E^1_{2g} mode can be split into two Raman modes by applying strain, the E^{1-}_{2g} mode (E'^- mode for monolayer) with a lower frequency and the E^{1+}_{2g} mode (E'^+ mode for monolayer) with a higher frequency.[43] In-plane tensile strain induces elongation of the lattice along the strain direction, leading to the redshift of E'^+ and E'^- modes for monolayer MoS_2, whereas the frequency change of the A_1' mode is not obvious (Figure S1) because the in-plane strain has a relatively small influence on the out-of-plane vibration.

The A exciton and B exciton have an energy difference of ~148 meV originating from the splitting of valence band caused by strong spin−orbit coupling.[44] Figure 1d shows the shift of the PL emission peak corresponding to A exciton with the increase of strain. When the uniaxial strain is applied, the conduction band at K point of Brillouin zone lowers,[45] resulting in the decrease of the band gap and the redshift of the A exciton peak, as shown in the inset of Figure 1e. Besides, the valence band at Γ point increases with the increase of strain, and the direct bandgap can change to an indirect one, leading to the appearance of an indirect transition peak (I).[34] The variation of the electronic band structure for monolayer MoS_2 under strain is calculated and shown in Figure S2.

https://doi.org/10.1021/acs.jpclett.1c03481
J. Phys. Chem. Lett. 2021, 12, 11555−11562

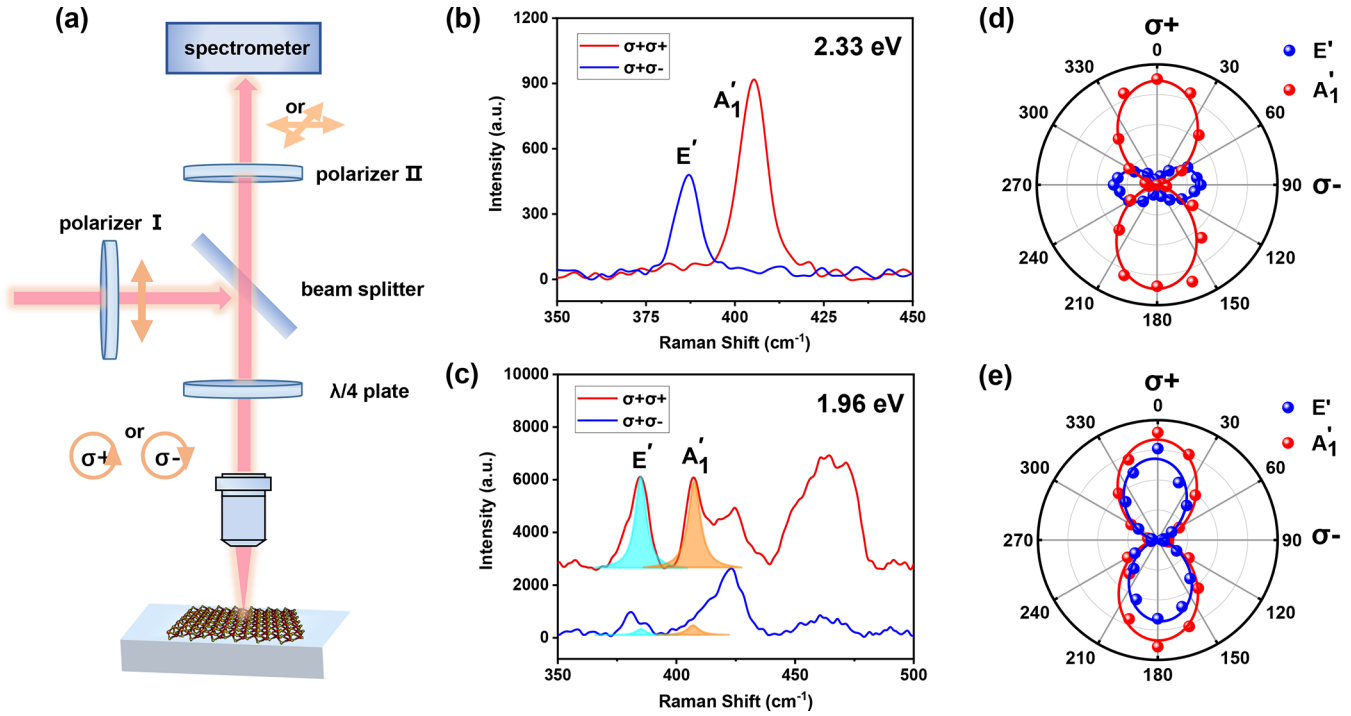

Figure 2. HRRS of monolayer MoS_2 for off- and on-excitonic resonance excitation. (a) The optical setup for HRRS. (b, c) The HRRS of monolayer MoS_2 excited by 2.33 eV (b) and 1.96 eV (c) lasers. The fitting and assignment of resonant Raman peaks in (c) are shown in Figure S4. (d, e) The polar plots of the intensities of E′ and A_1′ modes versus the rotation angle of the detected polarizer for the 2.33 eV (d) and 1.96 eV (e) laser excitation.

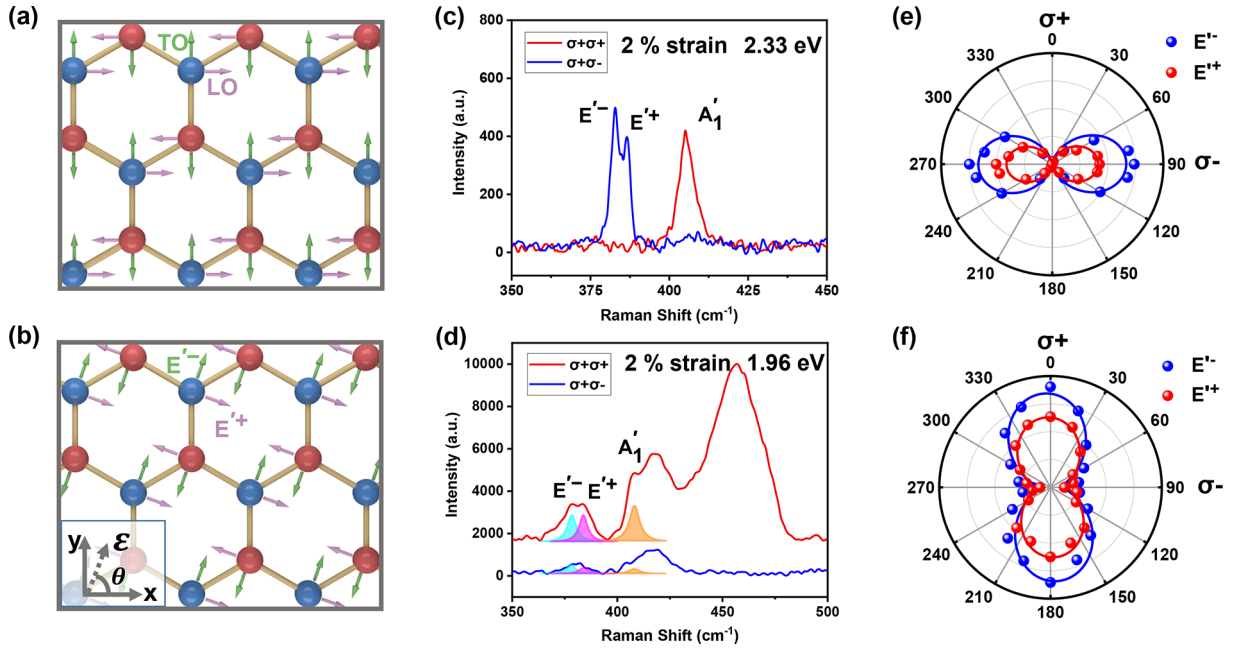

Figure 3. HRRS of strained MoS_2. (a, b) Schematic diagrams of the normal vibrations for the E′ mode of MoS_2 without strain (a) and for the E'^{-} and E'^{+} modes of strained MoS_2 (b). The inset of (b) shows the coordinate system for the crystal lattice and the direction of strain (ε). (c, d) HRRS of monolayer MoS_2 under 2% strain for the off-excitonic resonance excitation (2.33 eV) (c) and on-excitonic resonance excitation (1.96 eV) (d). (e, f) The polar plots of Raman intensities of E'^{-} and E'^{+} modes as a function of detected polarization angle for off-excitonic resonance excitation (2.33 eV) (e) and on-excitonic resonance excitation (1.96 eV) (f).

Figure 1e shows the increasing line width of the A exciton emission peak as a function of strain. At room temperature, the broadening of exciton emission is mainly due to the exciton−phonon coupling in MoS_2 under excitation of a 532 nm laser, and thus the variation of the line width of exciton emission peak can reflect the evolution of exciton−phonon coupling under strain.[25] The broadening of the A exciton peak indicates the enhanced exciton−phonon coupling. Both intravalley and intervalley scattering contribute to the total exciton−phonon coupling. The increase of exciton−phonon coupling in strained

https://doi.org/10.1021/acs.jpclett.1c03481
J. Phys. Chem. Lett. 2021, 12, 11555−11562

MoS_2 can be explained by the enhancement of intervalley phonon scattering ($e-p_{(K-\Gamma)}$) induced by the decreased band energy difference between K and Γ points, as schematically shown in Figure 1f. The enhancement of intervalley phonon scattering can also be evidenced by the decrease of valley polarization with increasing strain (Figure S3).

The HRRS is obtained by exciting the sample using circularly polarized light and collecting the Raman scattered light with the same ($\sigma+\sigma+$) or opposite ($\sigma+\sigma-$) helicity as the incident light. The optical setup is shown in Figure 2a. For MoS_2, the E′ mode is helicity-changed, and the A_1' mode is helicity-conserved for the off-excitonic resonance excitation (E_L = 2.33 eV), as shown in Figure 2b. The polar plot in Figure 2d shows the variation of Raman intensities of E′ and A_1' modes versus the detected polarization angle, which implies that the Raman scattered light for both modes are circularly polarized, whereas they have opposite helicities. However, the helicity selection rule of E′ mode changes when excited resonantly to the excitonic transition energies (E_L = 1.96 eV). Although the A_1' mode is still helicity-conserved, the E′ mode shows both helicity-conserved and helicity-changed components. Moreover, the helicity-conserved intensity is much larger than the helicity-changed intensity in monolayer MoS_2 (Figure 2c). It is seen from Figure 2e that the polarization state of the E′ mode is rotated by 90° compared with that in Figure 2d, which indicates that the E′ mode tends to have the same helicity as the A_1' mode. The change of helicity selection rule for on-excitonic resonance excitation can be attributed to the variation of dominant exciton−phonon coupling, which has been reported previously in semiconductors.[46,47]

The E′ mode of MoS_2 is a doubly degenerate Raman mode of the LO and TO phonons. The different helicity selection rules of the E′ mode for the off- and on-excitonic resonance excitations are related to the relative contributions of the DP and FI, which determine the intensities of the helicity-changed and helicity-conserved components, respectively (Note S1). For off-excitonic resonance excitation, DP is the dominant exciton−phonon coupling, and thus the helicity of the E′ mode is mainly changed, whereas for the on-excitonic resonance excitation the FI can be enhanced dramatically, resulting in the increased helicity-conserved Raman intensity. It is clear that the HRRS provides a method to separate the DP and FI and to explore the evolution of the proportion of the DP and FI under strain.

Figure 3a shows the normal vibrations of the degenerate LO and TO phonons for the E′ mode of primitive MoS_2. And Figure 3b shows the atomic vibrations of E'^- and E'^+ modes for strained MoS_2, which are parallel and perpendicular to the strain direction (ε), respectively. Figure 3c presents the HRRS of the E'^- and E'^+ modes of strained MoS_2 for off-excitonic resonance excitation (2.33 eV), and both E'^- and E'^+ modes are helicity-changed. The polar plot with rotating the detected polarization angle is shown in Figure 3e, which confirms that the polarization states of both E'^- and E'^+ modes are circularly polarized, and the helicity is opposite to the incident light. It has been reported that when the strained MoS_2 is excited by linearly polarized light, both E'^- and E'^+ modes are linearly polarized, and their polarization states are orthogonal.[38,48] From Figure 3c,e, it is seen that, when excited by circularly polarized light, the E'^- and E'^+ modes of MoS_2 have the same helicity. For on-excitonic resonance excitation (1.96 eV), as shown in Figure 3d, the helicity-conserved components of both E'^- and E'^+ modes dominate over the helicity-changed components. This is evidenced by the polar plot in Figure 3f, which shows the polarization states of these two modes are rotated by 90° compared with that in Figure 3e. The change of polarization states of both E'^- and E'^+ modes when excited resonantly to the excitonic states can also be attributed to the enhancement of the FI, as discussed previously.

The circularly polarized Raman intensity can be calculated by $I \propto |\sigma_s^{\dagger}\cdot R\cdot\sigma_i|^2$, where R is Raman tensor, σ_i and σ_s are the Jones vectors of incident and Raman scattered light. In the coordinate system as shown in Figure 3b, we set the zigzag and armchair direction of MoS_2 as the x and y axis. And the normal vibrations of LO and TO phonons for E′ mode are along the x and y axis, respectively. The FI induces diagonal components of the Raman tensor elements for the LO phonon,[49−51] and thus the Raman tensors of LO phonon and TO phonon for E′ mode can be expressed by

$$R_{LO} = \begin{pmatrix} f & d \\ d & f \end{pmatrix},\ R_{TO} = \begin{pmatrix} d & 0 \\ 0 & -d \end{pmatrix} \tag{1}$$

where d and f are the Raman tensor elements related to the DP and the FI, respectively. When the strain is applied along the direction of ε as shown in Figure 3b, the Raman tensors for the E'^- and E'^+ modes can be expressed by the linear combination of R_{LO} and R_{TO}[38,52]

$$R_{E'^-} = v_x^- R_{LO} + v_y^- R_{TO} \tag{2}$$

$$R_{E'^+} = v_x^+ R_{LO} + v_y^+ R_{TO} \tag{3}$$

where $v^- = \begin{pmatrix} \cos\theta \\ \sin\theta \end{pmatrix}$ and $v^+ = \begin{pmatrix} -\sin\theta \\ \cos\theta \end{pmatrix}$ are the unit vectors along the vibration directions of E'^- and E'^+ modes, respectively. θ is the angle between $\boldsymbol{\varepsilon}$ and the x axis.

Then the Raman intensities of helicity-conserved and helicity-changed components for E'^- and E'^+ modes under strain are calculated to be (see details in Note S2)

$$I_{E'^-}^{\sigma+\sigma+} \propto f^2 \cos^2\theta,\ I_{E'^-}^{\sigma+\sigma-} \propto d^2 \tag{4}$$

$$I_{E'^+}^{\sigma+\sigma+} \propto f^2 \sin^2\theta,\ I_{E'^+}^{\sigma+\sigma-} \propto d^2 \tag{5}$$

Thus, the helicity-conserved and helicity-changed intensities of both E'^- and E'^+ modes are only related to the FI and DP, respectively. For off-excitonic resonance excitation, the DP is much larger than the FI, and thus both E'^- and E'^+ modes are helicity-changed, whereas for on-excitonic resonance excitation, the FI is dramatically enhanced, and the helicity-conserved components of both E'^- and E'^+ modes can be larger than the helicity-changed components. Besides, the sum of the Raman intensities of E'^- and E'^+ modes in the $\sigma+\sigma+$ or $\sigma+\sigma-$ configurations are found to be $I_{sum}^{\sigma+\sigma+} \propto f^2$, $I_{sum}^{\sigma+\sigma-} \propto 2d^2$, which are equivalent to the expressions of $I_{\sigma+\sigma+}$ and $I_{\sigma+\sigma-}$ for the E′ mode of unstrained MoS_2 as shown in Note S1.

Considering that the intensity of helicity-changed component determined by DP is too weak to be detected in both unstrained and strained monolayer MoS_2, we use bilayer MoS_2 here to explore the evolution of DP and FI as a function of strain. The FI in bilayer MoS_2 is reduced compared with monolayer MoS_2 due to the dielectric screening effect.[37] The Raman and PL spectra of bilayer MoS_2 exhibit similar responses to strain as monolayer MoS_2, and the exciton−phonon coupling in bilayer MoS_2 is also enhanced under strain, as shown in Figure S5 and Figure S6. Besides, the

https://doi.org/10.1021/acs.jpclett.1c03481
J. Phys. Chem. Lett. 2021, 12, 11555−11562

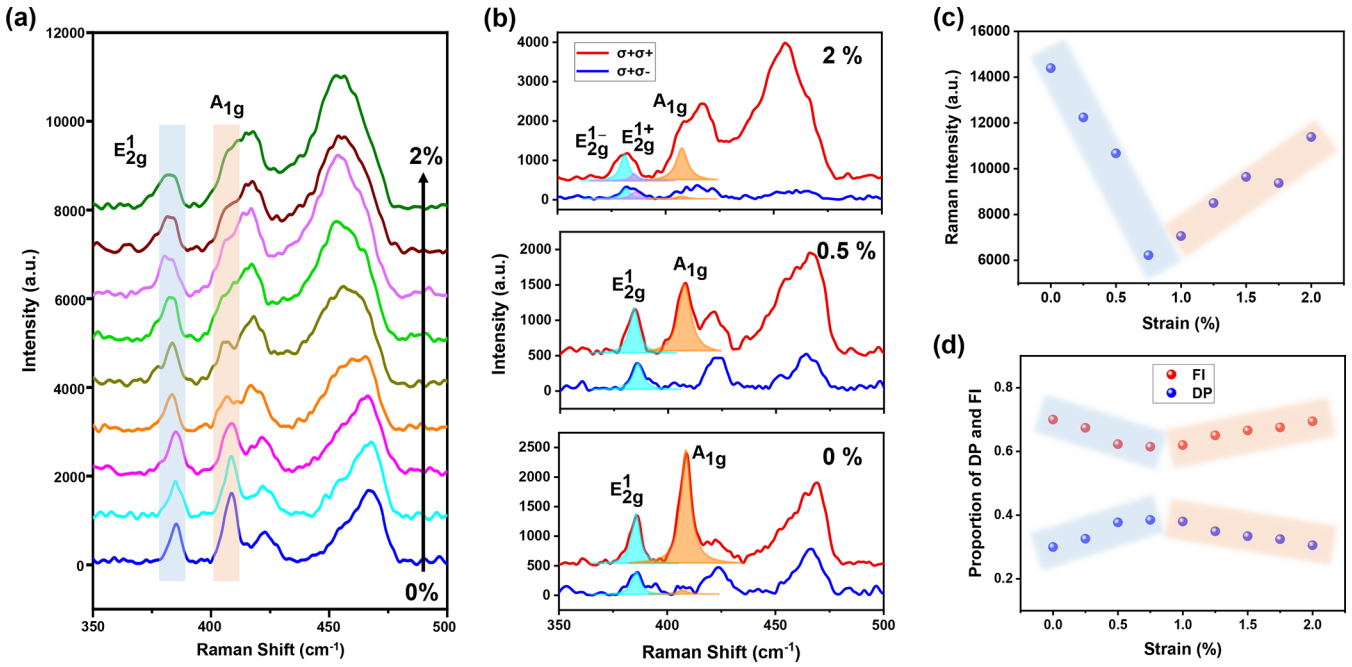

Figure 4. The variation of the FI and DP with the increase of strain. (a) The Raman spectra of bilayer MoS_2 as a function of strain, excited by a 1.96 eV laser. (b) HRRS of bilayer MoS_2 with 0%, 0.5%, and 2% strain, excited by a 1.96 eV laser. (c) The integral intensity of the A_{1g} mode as a function of strain. (d) The proportions of helicity-conserved and helicity-changed Raman intensities of the E^1_{2g} mode as a function of strain, which represent the proportion of the FI and DP, respectively. The blue and the orange regions in (c) and (d) represent the excitonic-resonance zone for the A and B excitons, respectively.

helicity selection rule analyzed above is also valid for strained bilayer MoS_2 (Figure S7).

Figure 4a displays the variation of resonant Raman intensity of bilayer MoS_2 with the increase of strain (E_L = 1.96 eV). The strain dependence of Raman intensities here can be attributed to the tuning of the resonance between the excitation laser energy and the excitonic transition energies. It has been reported that the intensity of A_{1g} mode is sensitive to the A and B excitons in MoS_2, whereas their influence on the E^1_{2g} mode is not obvious.[53,54] As shown in Figure 4a, the intensity of the E^1_{2g} mode changes slightly, whereas the intensity of the A_{1g} mode first decreases and then increases with the increase of strain, and the minimum of Raman intensity appears at ~0.75% strain (Figure 4c). The evolution of the A_{1g} mode can be explained by the variation of the excitonic resonance behavior. When the strain is applied, both the energies of A and B excitons redshift, and the excitation laser energy is first away from the resonance range of the A exciton and then approaches the resonance range of B exciton. The minimum intensity of the A_{1g} mode at ~0.75% strain means that the total excitonic resonance effect of A and B exciton reaches a minimum (Note S3, Figure S8). A similar trend is also observed by varying the temperature (Figure S9), which can also tune the excitonic resonance equivalently to the application of strain.

Figure 4b shows the HRRS of bilayer MoS_2 with the increase of strain. The helicity-conserved intensity of the E^1_{2g} mode (the sum of $I^{\sigma+\sigma+}_{E'^-}$ and $I^{\sigma+\sigma+}_{E'^+}$ for strained MoS_2) decreases when the excitation laser energy (E_L) is away from A exciton, and then it increases when the E_L approaches the B exciton, whereas the helicity-changed Raman intensity varies slightly (Figure S10), which indicates that the strength of FI is more sensitive to excitonic effects than DP. We further extract the proportions of helicity-conserved ($P_{\sigma+\sigma+}$) and helicity-changed ($P_{\sigma+\sigma-}$) components of the E^1_{2g} mode by $(I^{\sigma+\sigma+}_{sum})/(I^{\sigma+\sigma+}_{sum}+ I^{\sigma+\sigma-}_{sum})$ and $(I^{\sigma+\sigma-}_{sum})/(I^{\sigma+\sigma+}_{sum}+ I^{\sigma+\sigma-}_{sum})$, which represent the proportion of the FI and DP, respectively, as shown in Figure 4d. It is interesting that the proportion of FI also first decreases and then increases, consistent with the variation of the Raman intensity of the A_{1g} mode shown in Figure 4c.

The results above show that the FI is more sensitive to the excitonic resonance compared with DP, and the influence of strain on the proportion of the FI and DP is dominated by the excitonic effect. The exciton dependence of the FI and DP was previously reported theoretically in the semiconductor CdS,[51] which showed that both the FI and DP can be enhanced for excitonic resonance, but the FI can be enhanced much more than DP (see detail in Note S4). The remarkable exciton dependence of the strength of the FI can also be demonstrated by its variation with temperature (Figure S11). The increase of temperature not only induces the redshift of energies of A and B excitons but also induces the dissociation of excitons, which will greatly reduce the strength of the FI.

Strain is an efficient method to tune the excitonic energy states. When the uniaxial tensile strain is applied on layered MoS_2, both energies of A and B excitons redshift, resulting in the variation of resonance behavior between the excitation laser energy and the excitonic energy levels. The exciton−phonon coupling is also affected by the excitonic resonances, especially the proportion of the DP and FI. Benefiting from the special helicity selection rule of the E^1_{2g} mode that the helicity-conserved and helicity-changed Raman intensities are only determined by the FI and DP, respectively, we can separate the DP and FI in helicity-resolved Raman spectra and explore the exciton dependence of these two kinds of exciton−phonon couplings. The E^1_{2g} mode is split into two Raman modes under strain. We discussed the helicity selection rule of the E^{1+}_{2g} and E^{1-}_{2g} modes separately and used the sum of them to extract the proportion of helicity-conserved and helicity-changed compo-

https://doi.org/10.1021/acs.jpclett.1c03481
J. Phys. Chem. Lett. 2021, 12, 11555−11562

nents in order to compare with the unstrained case. Besides, the isotropic hexagonal crystal lattice becomes anisotropic when the uniaxial tensile strain is applied, and if excited by linearly polarized light, the optical response of strained MoS_2 will greatly depend on the crystalline orientation, making it complicated to study the exciton−phonon coupling using linearly polarized excitations. However, when circularly polarized excitation light is used for excitation, the crystalline orientation-dependence of optical response is eliminated. Hence, the circularly polarized Raman spectroscopy provides a unique method to study the exciton−phonon coupling in strained 2D materials.

In conclusion, we have demonstrated that the excitation laser energy first moves away from the resonance region of the A exciton and then approaches the resonance region of the B exciton with the increase of strain. The Raman intensities determined by the DP changes slightly, whereas the Raman intensities determined by the FI first decreases and then increases, which shows obvious dependence on the excitonic resonance. We conclude that although the line width of the PL emission peak increases monotonously with the increase of strain in MoS_2 which comprehensively reflects the increase of total intensity of the intravalley and intervalley exciton−phonon interactions, the strength of intravalley DP and FI may not vary monotonously, depending on the excitonic resonance effect. Our work provides more detailed research on the evolution of different kinds of exciton−phonon couplings under strain and demonstrates the exciton dependence of the DP and FI. The method can also be extended to other 2D semiconductors and would be helpful for the manipulation of exciton−phonon couplings.

■ ASSOCIATED CONTENT

Supporting Information

The Supporting Information is available free of charge at https://pubs.acs.org/doi/10.1021/acs.jpclett.1c03481.

Characterization methods of Raman scattering and photoluminescence spectroscopy; helicity selection rule for unstrained and strained MoS_2; analysis of the variation of excitonic resonance with the increase of strain; the influence of temperature on the relative proportion of DP and FI (PDF)

■ AUTHOR INFORMATION

Corresponding Author

Lianming Tong − *College of Chemistry and Molecular Engineering, Beijing Science and Engineering Center for Nanocarbons, Beijing National Laboratory for Molecular Sciences,, Peking University, Beijing 100871, P. R. China;* orcid.org/0000-0001-7771-4077; Email: tonglm@pku.edu.cn

Authors

Yan Zhao − *Academy for Advanced Interdisciplinary Studies, Peking University, Beijing 100871, P. R. China; College of Chemistry and Molecular Engineering, Beijing Science and Engineering Center for Nanocarbons, Beijing National Laboratory for Molecular Sciences,, Peking University, Beijing 100871, P. R. China*

Shuqing Zhang − *Institute of Information Photonics Technology, Faculty of Science, Beijing University of Technology, Beijing 100124, P. R. China*

Bo Xu − *Academy for Advanced Interdisciplinary Studies, Peking University, Beijing 100871, P. R. China; College of Chemistry and Molecular Engineering, Beijing Science and Engineering Center for Nanocarbons, Beijing National Laboratory for Molecular Sciences,, Peking University, Beijing 100871, P. R. China*

Shishu Zhang − *College of Chemistry and Molecular Engineering, Beijing Science and Engineering Center for Nanocarbons, Beijing National Laboratory for Molecular Sciences,, Peking University, Beijing 100871, P. R. China*

Shiyi Han − *College of Chemistry and Molecular Engineering, Beijing Science and Engineering Center for Nanocarbons, Beijing National Laboratory for Molecular Sciences,, Peking University, Beijing 100871, P. R. China*

Jin Zhang − *College of Chemistry and Molecular Engineering, Beijing Science and Engineering Center for Nanocarbons, Beijing National Laboratory for Molecular Sciences,, Peking University, Beijing 100871, P. R. China;* orcid.org/0000-0003-3731-8859

Complete contact information is available at: https://pubs.acs.org/10.1021/acs.jpclett.1c03481

Author Contributions

Y.Z. conceived the idea and designed the experiments. S.Z. calculated the electronic band structures of MoS_2. B.X., S.Z., and S.H. coordinated the measurement of helicity-resolved Raman spectra. Y.Z. wrote the manuscript. The work was supervised by L.T. and J.Z. All the authors discussed the results and commented on the manuscript.

Notes

The authors declare no competing financial interest.

■ ACKNOWLEDGMENTS

This work was financially supported by the Ministry of Science and Technology of China (2018YFA0703502 and 2016YFA0200104) and the National Natural Science Foundation of China (Grant Nos. 51720105003, 21790052, 52021006, and 21974004), the Strategic Priority Research Program of CAS (XDB36030100), and the Beijing National Laboratory for Molecular Sciences (BNLMS-CXTD-202001). S.Q. Zhang was supported by the Open Research Fund of CNMGE Platform & NSCC-TJ.

■ REFERENCES

(1) Roldan, R.; Castellanos-Gomez, A.; Cappelluti, E.; Guinea, F. Strain Engineering in Semiconducting Two-Dimensional Crystals. *J. Phys.: Condens. Matter* **2015**, *27*, 313201.

(2) Castellanos-Gomez, A.; Roldan, R.; Cappelluti, E.; Buscema, M.; Guinea, F.; van der Zant, H. S. J.; Steele, G. A. Local Strain Engineering in Atomically Thin MoS_2. *Nano Lett.* **2013**, *13*, 5361−5366.

(3) Dai, Z.; Liu, L.; Zhang, Z. Strain Engineering of 2D Materials: Issues and Opportunities at the Interface. *Adv. Mater.* **2019**, *31*, 1805417.

(4) Maiti, R.; Patil, C.; Saadi, M. A. S. R.; Xie, T.; Azadani, J. G.; Uluutku, B.; Amin, R.; Briggs, A. F.; Miscuglio, M.; Van Thourhout, D.; Solares, S. D.; Low, T.; Agarwal, R.; Bank, S. R.; Sorger, V. J. Strain-Engineered High-Responsivity $MoTe_2$ Photodetector for Silicon Photonic Integrated Circuits. *Nat. Photonics* **2020**, *14*, 578−584.

(5) Fei, R.; Yang, L. Strain-Engineering the Anisotropic Electrical Conductance of Few-Layer Black Phosphorus. *Nano Lett.* **2014**, *14*, 2884−2889.

(6) Shi, H.; Pan, H.; Zhang, Y.-W.; Yakobson, B. I. Quasiparticle Band Structures and Optical Properties of Strained Monolayer MoS_2 and WS_2. *Phys. Rev. B: Condens. Matter Mater. Phys.* **2013**, *87*, 155304.
(7) Ge, Y.; Wan, W.; Feng, W.; Xiao, D.; Yao, Y. Effect of Doping and Strain Modulations on Electron Transport in Monolayer MoS_2. *Phys. Rev. B: Condens. Matter Mater. Phys.* **2014**, *90*, 035414.
(8) Chen, Y.; Deng, W.; Chen, X.; Wu, Y.; Shi, J.; Zheng, J.; Chu, F.; Liu, B.; An, B.; You, C.; Jiao, L.; Liu, X.; Zhang, Y. Carrier Mobility Tuning of MoS_2 by Strain Engineering in CVD Growth Process. *Nano Res.* **2021**, *14*, 2314−2320.
(9) Xiao, X.; Wu, M.; Ni, Z.; Xu, S.; Chen, S.; Hu, J.; Rudd, P. N.; You, W.; Huang, J. Ultrafast Exciton Transport with a Long Diffusion Length in Layered Perovskites with Organic Cation Functionalization. *Adv. Mater.* **2020**, *32*, 2004080.
(10) Aslan, O. B.; Deng, M.; Heinz, T. F. Strain Tuning of Excitons in Monolayer WSe_2. *Phys. Rev. B: Condens. Matter Mater. Phys.* **2018**, *98*, 115308.
(11) Aslan, O. B.; Datye, I. M.; Mleczko, M. J.; Cheung, K. S.; Krylyuk, S.; Bruma, A.; Kalish, I.; Davydov, A. V.; Pop, E.; Heinz, T. F. Probing the Optical Properties and Strain-Tuning of Ultrathin $Mo_{1-x}W_xTe_2$. *Nano Lett.* **2018**, *18*, 2485−2491.
(12) Aslan, O. B.; Deng, M.; Brongersma, M. L.; Heinz, T. F. Strained Bilayer WSe_2 with Reduced Exciton-Phonon Coupling. *Phys. Rev. B: Condens. Matter Mater. Phys.* **2020**, *101*, 115305.
(13) Prunnila, M.; Kivinen, P.; Savin, A.; Torma, P.; Ahopelto, J. Intervalley-Scattering-Induced Electron-Phonon Energy Relaxation in Many-Valley Semiconductors at Low Temperatures. *Phys. Rev. Lett.* **2005**, *95*, 206602.
(14) Chen, C.; Chen, X.; Yu, H.; Shao, Y.; Guo, Q.; Deng, B.; Lee, S.; Ma, C.; Watanabe, K.; Taniguchi, T.; Park, J.-G.; Huang, S.; Yao, W.; Xia, F. Symmetry-Controlled Electron-Phonon Interactions in van der Waals Heterostructures. *ACS Nano* **2019**, *13*, 552−559.
(15) Herbert, D. C. Electron-Phonon Interaction and Inter-Valley Scattering in Semiconductors. *J. Phys. C: Solid State Phys.* **1973**, *6*, 2788−2810.
(16) Ersfeld, M.; Volmer, F.; de Melo, P. M. M. C.; de Winter, R.; Heithoff, M.; Zanolli, Z.; Stampfer, C.; Verstraete, M. J.; Beschoten, B. Spin States Protected from Intrinsic Electron-Phonon Coupling Reaching 100 ns Lifetime at Room Temperature in $MoSe_2$. *Nano Lett.* **2019**, *19*, 4083−4090.
(17) Yu, Z.; Ong, Z.-Y.; Li, S.; Xu, J.-B.; Zhang, G.; Zhang, Y.-W.; Shi, Y.; Wang, X. Analyzing the Carrier Mobility in Transition-Metal Dichalcogenide MoS_2 Field-Effect Transistors. *Adv. Funct. Mater.* **2017**, *27*, 1604093.
(18) Yang, F.; Wu, J.; Suwardi, A.; Zhao, Y.; Liang, B.; Jiang, J.; Xu, J.; Chi, D.; Hippalgaonkar, K.; Lu, J.; Ni, Z. Gate-Tunable Polar Optical Phonon to Piezoelectric Scattering in Few-Layer Bi_2O_2Se for High-Performance Thermoelectrics. *Adv. Mater.* **2021**, *33*, 2004786.
(19) Liao, B.; Qiu, B.; Zhou, J.; Huberman, S.; Esfarjani, K.; Chen, G. Significant Reduction of Lattice Thermal Conductivity by the Electron-Phonon Interaction in Silicon with High Carrier Concentrations: A First-Principles Study. *Phys. Rev. Lett.* **2015**, *114*, 115901.
(20) Sohier, T.; Gibertini, M.; Campi, D.; Pizzi, G.; Marzari, N. Valley-Engineering Mobilities in Two-Dimensional Materials. *Nano Lett.* **2019**, *19*, 3723−3729.
(21) Bardeen, J.; Shockley, W. Deformation Potentials and Mobilities in Non-Polar Crystals. *Phys. Rev.* **1950**, *80*, 72−80.
(22) Fröhlich, H. Interaction of Electrons with Lattice Vibrations. *Proc. R. Soc. London A* **1952**, *215*, 291−298.
(23) Chernikov, A.; Bornwasser, V.; Koch, M.; Chatterjee, S.; Boettge, C. N.; Feldtmann, T.; Kira, M.; Koch, S. W.; Wassner, T.; Lautenschlaeger, S.; Meyer, B. K.; Eickhoff, M. Phonon-Assisted Luminescence of Polar Semiconductors: Fröhlich Coupling *versus* Deformation-Potential Scattering. *Phys. Rev. B: Condens. Matter Mater. Phys.* **2012**, *85*, 035201.
(24) Fu, M.; Tamarat, P.; Trebbia, J.-B.; Bodnarchuk, M. I.; Kovalenko, M. V.; Even, J.; Lounis, B. Unraveling Exciton-Phonon Coupling in Individual $FAPbI_3$ Nanocrystals Emitting Near-Infrared Single Photons. *Nat. Commun.* **2018**, *9*, 3318.
(25) Niehues, I.; Schmidt, R.; Druppel, M.; Marauhn, P.; Christiansen, D.; Selig, M.; Berghauser, G.; Wigger, D.; Schneider, R.; Braasch, L.; Koch, R.; Castellanos-Gomez, A.; Kuhn, T.; Knorr, A.; Malic, E.; Rohlfing, M.; Michaelis de Vasconcellos, S.; Bratschitsch, R. Strain Control of Exciton-Phonon Coupling in Atomically Thin Semiconductors. *Nano Lett.* **2018**, *18*, 1751−1757.
(26) Ho, C. H.; Wu, C. S.; Huang, Y. S.; Liao, P. C.; Tiong, K. K. Temperature Dependence of Energies and Broadening Parameters of the Band-Edge Excitons of $Mo_{1-x}W_xS_2$ Single Crystals. *J. Phys.: Condens. Matter* **1998**, *10*, 9317−9328.
(27) Shen, W. Z.; Tang, W. G.; Li, Z. Y.; Shen, S. C.; Andersson, T. Exciton Line Broadening in Strained InGaAs/GaAs Single Quantum Wells. *Appl. Phys. A: Mater. Sci. Process.* **1995**, *60*, 243−245.
(28) Steele, J. A.; Puech, P.; Keshavarz, M.; Yang, R.; Banerjee, S.; Debroye, E.; Kim, C. W.; Yuan, H.; Heo, N. H.; Vanacken, J.; Walsh, A.; Hofkens, J.; Roeffaers, M. B. J. Giant Electron-Phonon Coupling and Deep Conduction Band Resonance in Metal Halide Double Perovskite. *ACS Nano* **2018**, *12*, 8081−8090.
(29) Yan, B.; Chen, R.; Zhou, W.; Zhang, J.; Sun, H.; Gong, H.; Yu, T. Localized Suppression of Longitudinal-Optical-Phonon-Exciton Coupling in Bent ZnO Nanowires. *Nanotechnology* **2010**, *21*, 445706.
(30) Komsa, H.-P.; Krasheninnikov, A. V. Effects of Confinement and Environment on the Electronic Structure and Exciton Binding Energy of MoS_2 from First Principles. *Phys. Rev. B: Condens. Matter Mater. Phys.* **2012**, *86*, 241201.
(31) Mak, K. F.; Lee, C.; Hone, J.; Shan, J.; Heinz, T. F. Atomically Thin MoS_2: A New Direct-Gap Semiconductor. *Phys. Rev. Lett.* **2010**, *105*, 136805.
(32) Splendiani, A.; Sun, L.; Zhang, Y.; Li, T.; Kim, J.; Chim, C.-Y.; Galli, G.; Wang, F. Emerging Photoluminescence in Monolayer MoS_2. *Nano Lett.* **2010**, *10*, 1271−1275.
(33) He, K.; Poole, C.; Mak, K. F.; Shan, J. Experimental Demonstration of Continuous Electronic Structure Tuning *via* Strain in Atomically Thin MoS_2. *Nano Lett.* **2013**, *13*, 2931−2936.
(34) Conley, H. J.; Wang, B.; Ziegler, J. I.; Haglund, R. F., Jr.; Pantelides, S. T.; Bolotin, K. I. Bandgap Engineering of Strained Monolayer and Bilayer MoS_2. *Nano Lett.* **2013**, *13*, 3626−3630.
(35) Peelaers, H.; Van de Walle, C. G. Effects of Strain on Band Structure and Effective Masses in MoS_2. *Phys. Rev. B: Condens. Matter Mater. Phys.* **2012**, *86*, 241401.
(36) Miller, B.; Lindlau, J.; Bommert, M.; Neumann, A.; Yamaguchi, H.; Holleitner, A.; Hoegele, A.; Wurstbauer, U. Tuning the Fröhlich Exciton-Phonon Scattering in Monolayer MoS_2. *Nat. Commun.* **2019**, *10*, 807.
(37) Zhao, Y.; Zhang, S.; Shi, Y.; Zhang, Y.; Saito, R.; Zhang, J.; Tong, L. Characterization of Excitonic Nature in Raman Spectra Using Circularly Polarized Light. *ACS Nano* **2020**, *14*, 10527−10535.
(38) Wang, Y.; Cong, C.; Qiu, C.; Yu, T. Raman Spectroscopy Study of Lattice Vibration and Crystallographic Orientation of Monolayer MoS_2 under Uniaxial Strain. *Small* **2013**, *9*, 2857−2861.
(39) Ni, Z. H.; Yu, T.; Lu, Y. H.; Wang, Y. Y.; Feng, Y. P.; Shen, Z. X. Uniaxial Strain on Graphene: Raman Spectroscopy Study and Band-Gap Opening. *ACS Nano* **2008**, *2*, 2301−2305.
(40) Liu, Z.; Amani, M.; Najmaei, S.; Xu, Q.; Zou, X.; Zhou, W.; Yu, T.; Qiu, C.; Birdwell, A. G.; Crowne, F. J.; Vajtai, R.; Yakobson, B. I.; Xia, Z.; Dubey, M.; Ajayan, P. M.; Lou, J. Strain and Structure Heterogeneity in MoS_2 Atomic Layers Grown by Chemical Vapour Deposition. *Nat. Commun.* **2014**, *5*, 5246.
(41) Lim, J. H.; Ratnam, M. M.; Azid, I. A.; Mutharasu, D. Determination of Young's Modulus of Epoxy Coated Polyethylene Micro-Cantilever Using Phase-Shift Shadow Moire Method. *Opt. Lasers Eng.* **2011**, *49*, 1301−1308.
(42) Lee, C.; Yan, H.; Brus, L. E.; Heinz, T. F.; Hone, J.; Ryu, S. Anomalous Lattice Vibrations of Single- and Few-Layer MoS_2. *ACS Nano* **2010**, *4*, 2695−2700.
(43) Mohiuddin, T. M. G.; Lombardo, A.; Nair, R. R.; Bonetti, A.; Savini, G.; Jalil, R.; Bonini, N.; Basko, D. M.; Galiotis, C.; Marzari, N.; Novoselov, K. S.; Geim, A. K.; Ferrari, A. C. Uniaxial Strain in Graphene by Raman Spectroscopy: G Peak Splitting, Gruneisen

https://doi.org/10.1021/acs.jpclett.1c03481
J. Phys. Chem. Lett. 2021, 12, 11555−11562

Parameters, and Sample Orientation. *Phys. Rev. B: Condens. Matter Mater. Phys.* **2009**, *79*, 205433.
(44) Zhu, Z. Y.; Cheng, Y. C.; Schwingenschlögl, U. Giant Spin-Orbit-Induced Spin Splitting in Two-Dimensional Transition-Metal Dichalcogenide Semiconductors. *Phys. Rev. B: Condens. Matter Mater. Phys.* **2011**, *84*, 153402.
(45) Kumar, A.; Ahluwalia, P. K. Mechanical Strain Dependent Electronic and Dielectric Properties of Two-Dimensional Honeycomb Structures of MoX_2 (X = S, Se, Te). *Phys. B* **2013**, *419*, 66−75.
(46) Martin, R. M.; Damen, T. C. Breakdown of Selection Rules in Resonance Raman Scattering. *Phys. Rev. Lett.* **1971**, *26*, 86−88.
(47) Tan, Q.-H.; Sun, Y.-J.; Liu, X.-L.; Xu, K.-X.; Gao, Y.-F.; Ren, S.-L.; Tan, P.-H.; Zhang, J. Breakdown of Raman Selection Rules by Fröhlich Interaction in Few-Layer WS_2. *Nano Res.* **2021**, *14*, 239−244.
(48) Doratotaj, D.; Simpson, J. R.; Yan, J.-A. Probing the Uniaxial Strains in MoS_2 Using Polarized Raman Spectroscopy: A First-Principles Study. *Phys. Rev. B: Condens. Matter Mater. Phys.* **2016**, *93*, 075401.
(49) Trallero-Giner, C.; Cantarero, A.; Cardona, M. One-Phonon Resonant Raman Scattering: Fröhlich Exciton-Phonon Interaction. *Phys. Rev. B: Condens. Matter Mater. Phys.* **1989**, *40*, 4030−4036.
(50) Cantarero, A.; Trallero-Giner, C.; Cardona, M. Excitons in One-Phonon Resonant Raman Scattering: Fröhlich and Interference Effects. *Phys. Rev. B: Condens. Matter Mater. Phys.* **1989**, *40*, 12290−12295.
(51) Martin, R. M. Theory of the One-Phonon Resonance Raman Effect. *Phys. Rev. B* **1971**, *4*, 3676−3685.
(52) Huang, M.; Yan, H.; Chen, C.; Song, D.; Heinz, T. F.; Hone, J. Phonon Softening and Crystallographic Orientation of Strained Graphene Studied by Raman Spectroscopy. *Proc. Natl. Acad. Sci. U. S. A.* **2009**, *106*, 7304−7308.
(53) Carvalho, B. R.; Malard, L. M.; Alves, J. M.; Fantini, C.; Pimenta, M. A. Symmetry-Dependent Exciton-Phonon Coupling in 2D and Bulk MoS_2 Observed by Resonance Raman Scattering. *Phys. Rev. Lett.* **2015**, *114*, 136403.
(54) Livneh, T.; Sterer, E. Resonant Raman Scattering at Exciton States Tuned by Pressure and Temperature in 2H-MoS_2. *Phys. Rev. B: Condens. Matter Mater. Phys.* **2010**, *81*, 195209.

https://doi.org/10.1021/acs.jpclett.1c03481
J. Phys. Chem. Lett. 2021, 12, 11555−11562